International Journal of Nanomedicine

Dovepress
Taylor & Francis Group

Open Access Full Text Article

ORIGINAL RESEARCH

Pulmonary Exposure to Copper Oxide Nanoparticles Induces Systemic Inflammation, Oxidative Stress, and Prothrombotic Responses in BALB/c Mice

Zannatul Ferdous[1,2], Sumaya Beegam[1], Nur Elena Zaaba[1], Ozaz Elzaki[1], Yaser E Greish[3], Abderrahim Nemmar[1,4]

[1]Department of Physiology, College of Medicine and Health Sciences, United Arab Emirates University, Al-Ain, United Arab Emirates; [2]Department of Biological Sciences, Sunnybrook Research Institute, Toronto, ON, Canada; [3]Department of Chemistry, College of Science, United Arab Emirates University, Al Ain, United Arab Emirates; [4]Zayed Center for Health Sciences, United Arab Emirates University, Al-Ain, United Arab Emirates

Correspondence: Abderrahim Nemmar, Department of Physiology, College of Medicine and Health Sciences, United Arab Emirates University, Al-Ain, 15551, United Arab Emirates, Email anemmar@uaeu.ac.ae

Introduction: Copper oxide nanoparticles (CuONPs) are increasingly used in industrial and biomedical applications; however, their potential to provoke systemic vascular and hemostatic disturbances remains poorly defined.

Methods: BALB/c mice were subjected to a single pulmonary instillation of CuONPs at doses of 3 µg or 30 µg per mouse, and the endpoints were evaluated 24 h post-exposure. Prior to biological testing, the CuONPs were characterized by X-ray diffraction, dynamic light scattering, zeta potential analyses and transmission electron microscopy, confirming their high crystallinity, relatively uniform particle size distribution and good electrostatic stability.

Results: Exposure to CuONPs significantly shortened the thrombotic occlusion times in arterioles and venules; reduced prothrombin and activated partial thromboplastin times; and elevated plasma platelet factor 4, fibrinogen, plasminogen activator inhibitor-1, and C-reactive protein levels, indicating a shift toward a prothrombotic state. Oxidative stress is evidenced by increased levels of thiobarbituric acid-reactive substances, depleted glutathione levels, and decreased nitric oxide levels. In parallel, CuONPs induced significant upregulation of pro-inflammatory cytokines (tumor necrosis factor-α, interleukin (IL)-6, and IL-1β) and markers of DNA damage and apoptosis, including 8-hydroxy-2′-deoxyguanosine, cytochrome C release, and cleaved caspase-3 expression.

Discussion: Collectively, these findings demonstrated that pulmonary exposure to low and high doses of CuONPs triggered systemic oxidative stress and inflammation, leading to prothrombotic responses, DNA damage, and apoptosis. This study highlights the potential vascular risks associated with CuONPs and underscores the importance of careful safety evaluation in biomedical and environmental contexts.

Keywords: copper oxide nanoparticles, pulmonary exposure, oxidative stress, inflammation, thrombosis

Introduction

The use of nanotechnology, which encompasses the design, production, and application of materials at the nanoscale, has increased substantially in recent years. This growth is primarily driven by the unique physical, chemical, and biological properties of nanoparticles, which are largely attributed to their high surface area and quantum effects.[1,2] Consequently, nanoparticles have found extensive applications in medicine (eg, targeted drug delivery and diagnostic imaging), electronics (eg, smaller and more efficient devices), environmental protection (eg, water purification and pollution control), and agriculture (eg, nanofertilizers and pesticides).[3]

Among the diverse nanomaterials produced, metallic nanoparticles synthesized from Cu, Zn, Ti, Mg, Au, alginate, and Ag are particularly noteworthy. Copper oxide nanoparticles (CuONPs) are among the most prominent inorganic

https://doi.org/10.2147/IJN.S579331
Received: 16 December 2025
Accepted: 16 May 2026
Published: 16 June 2026

metal-oxide nanomaterials. Copper is an essential trace element in humans and animals, playing a critical role in connective tissue cross-linking, as well as in iron and lipid metabolism.[4] In addition, copper is naturally present in the environment through geological sources and anthropogenic emissions, including mining, smelting, combustion, and industrial waste.[5] It exists in multiple forms, including zero-valent, ionic, and nanoparticulate states. All these cupric forms exhibit differential levels of toxicity across biological systems. Engineered CuONPs are increasingly released into the environment through wastewater effluents and agricultural systems, raising concerns regarding their environmental persistence and biological impact.[6]

Human exposure to CuONPs occurs primarily in occupational and environmental settings. Workers involved in nanoparticle synthesis, processing, packaging, and transportation are at increased risk, particularly in industries such as asphalt and rubber manufacturing.[7] Inhalation represents the predominant route of exposure, although ingestion, dermal absorption, and ocular contact may also contribute.[7] Following inhalation, nanoparticles can deposit throughout the respiratory tract depending on their size, translocate across alveolar-capillary barrier, and enter systemic circulation. In this regard, we and others have previously shown that pulmonary exposed nanoparticles can pass into the bloodstream and distribute to major organs, including the brain, kidney, heart and liver.[8–11]

The biodistribution of nanoparticles has been associated with a range of biological responses, including oxidative stress, inflammation, DNA damage, and apoptosis, with oxidative stress recognized as a key underlying mechanism of CuONPs-induced toxicity.[12] A growing body of literature has explored CuONPs toxicity using both in vitro and in vivo models. In vitro studies have demonstrated cytotoxic effects in human lung epithelial, endothelial, renal, and neuronal cells, while in vivo studies have reported neurobehavioral impairments, altered locomotion, and developmental toxicity in animal models.[13–18] Increasing experimental evidence highlights the pulmonary toxicity of CuONPs following inhalation exposure. For instance, CuONPs have been shown to induce dose-dependent pulmonary inflammation, epithelial cell apoptosis, and oxidative stress, with increased reactive oxygen species (ROS) contributing to cellular injury.[19] In addition, exposure has been associated with collagen deposition and upregulation of α-smooth muscle actin, suggesting a potential role in the development of pulmonary fibrosis.[20] Sub-acute inhalation studies further demonstrate sustained inflammatory responses and dynamic clearance kinetics, with copper persisting in lung tissue and exhibiting a measurable half-life.[21] Importantly, inhaled CuONPs have been shown to translocate beyond the lungs, leading to increased copper levels in systemic circulation and secondary organs such as the heart, kidneys, and spleen, indicating the potential for multi-organ effects following respiratory exposure.[21] Despite these findings, quantitative data on human exposure levels and established toxic thresholds, particularly for inhalation exposure, remain limited, hindering accurate risk assessment.

Metallic nanoparticles have also been investigated for pulmonary delivery due to their potential advantages, including targeted deposition and controlled release.[22,23] However, these benefits must be balanced against concerns regarding toxicity, biopersistence, and unintended systemic distribution. CuONPs are of particular interest given their widespread industrial use, high likelihood of inhalation exposure, and strong redox activity, which may amplify biological responses.[5] Notably, the toxic dose of copper nanoparticles, including zero-valent copper and copper(I) oxide, has been reported to be up to ten times lower than that of ionic copper in some plants, aquatic organisms, rodents, and cell cultures, indicating greater cytotoxicity.[5,24] And this property has been exploited in recent studies that proposed CuONPs as potential drug carriers for chemotherapy.[23,25]

While previous studies have reported pulmonary inflammation and organ-specific toxicity associated with CuONPs, a comprehensive evaluation of their acute systemic effects following pulmonary exposure remains lacking. In particular, the extent to which pulmonary exposure contributes to downstream thrombotic, inflammatory, and genotoxic responses is not fully understood. Therefore, the present study aimed to investigate the acute systemic effects of CuONPs following pulmonary administration, with a specific focus on thrombotic events, systemic inflammation, oxidative stress, DNA damage, and apoptosis using both in vivo and in vitro models. By addressing these endpoints, our work seeks to advance understanding of CuONPs-induced toxicity and support future risk assessment and safe application of these nanomaterials.

Materials and Methods

Characterization of CuONPs

Dry black powder of spherical CuONPs was purchased from PlasmaChem (Schwarzschild St., Berlin, Germany). The average particle size of the powder was 15–50 nm with a purity of >97%, according to the manufacturer.

Physicochemical characterization of CuONPs was conducted to confirm their crystalline structures, particle size distributions, and surface charge properties. The crystalline phase and structural purity of the CuONPs were analyzed by X-ray diffraction (XRD). The XRD pattern was recorded using Cu Kα radiation (λ = 1.5406 Å) over the 2θ range of 20–80°. The diffraction peaks were compared with Joint Committee on Powder Diffraction Standards (JCPDS) card no. 01-080-0076 to identify the characteristic diffraction planes corresponding to the monoclinic phase of CuO. The particle size distribution of the CuONPs was measured by dynamic light scattering (DLS) on a Zetasizer Nano ZS (Malvern Instruments, UK). Prior to measurement, the nanoparticles were ultrasonically dispersed in deionized water to minimize agglomeration. The zeta potential of the CuONPs suspension was determined using a Zetasizer Nano ZS instrument to evaluate surface charge and colloidal stability. Measurements were performed at 25 °C in aqueous suspension at neutral pH. All characterization procedures were carried out under controlled laboratory conditions following standard protocols reported in the literature.[26,27] CuONPs were further characterized for their morphology, particle size and particle size distribution using a transmission electron microscopy (TEM; Thermo Scientific Talos F200i). The well-suspended CuONPs were immobilized on a Copper mesh with 400 µm Carbon Film. A TEM Bright Field Image at 50 nm resolution, 5-second exposure, spot size 5 was recorded.

CuONPs were suspended in sterile saline (0.9% NaCl). To reduce nanoparticle aggregation, suspensions of CuONPs were sonicated (Clifton Ultrasonic Bath, Clifton, NJ, USA) for 10 min and vortexed prior to dilution and intratracheal (i.t.) instillation.

Animals and Dosing

BALB/C mice, aged 8–10 weeks, with an equal distribution of males and females, weighing 25 to 30g (Animal House of the College of Medicine and Health Sciences, United Arab Emirates University) were housed in light- (12 h light: 12 h dark cycle) and temperature-controlled (22 ± 1°C) room. They had free access to commercial laboratory chow and tap water.

Pulmonary exposure was achieved by intratracheal (i.t.) instillation.[9,28] Mice were anesthetized with isoflurane and positioned supine with an extended neck on an angled board. A Becton Dickinson 24 Gauge cannula was introduced into the trachea via the mouth. A single dose of CuONPs (3 µg or 30 µg per mouse) or saline (control) was administered (100 µL) using a sterile syringe, followed by an equal volume of an air bolus. Twenty-four hours after i.t. instillation of saline or CuONPs, the mice were anesthetized using an intraperitoneal (i.p.) injection of sodium pentobarbital (45 mg/kg), after which blood was collected from the inferior vena cava in 4% EDTA and centrifuged at 4 °C for 15 min at 900 g. The plasma samples obtained were stored at −80 °C as they awaited analysis, and various parameters of oxidative stress, inflammation, DNA damage, and apoptosis were assessed.

This study was reviewed and approved by the United Arab Emirates University Animal Ethics Committee (approval # ERA_2019_5876), and all experiments were conducted in accordance with the approved protocols and in compliance with the *Guide for the Care and Use of Laboratory Animals (National Research Council, 8th edition, 2011).*

Experimental Pial Arterioles and Venules Thrombosis Model

In separate sets of animals, in vivo thrombogenesis in the pial arterioles and venules was assessed in BALB/c mice after saline or CuONPs exposure for 24 h according to a previously described technique.[9] Briefly, the animals were anesthetized with urethane (1 mg/g BW, i.p.)., the trachea was intubated, and the right jugular vein was cannulated with a 2F venous catheter (Portex, Hythe, UK) for fluorescein administration (Sigma, St. Louis, MO, USA). Thereafter, craniotomy was performed on the right temporoparietal cortex with a handheld microdrill, and the dura was stripped open. Only untraumatized preparations were used, and those showing trauma to either the microvessels or the underlying brain tissue were discarded. Cerebral microcirculation was directly visualized using a fluorescence microscope

(Olympus, Melville, NY, USA) connected to a camera and DVD recorder. A heating pad was used, and body temperature was raised to 37°C, as monitored using a rectal thermoprobe connected to a temperature reader (Physitemp Instruments, NJ, USA). A field containing arterioles and venules of 15–20 μm in diameter was selected. Such a field was taped prior to, and during the photochemical insult, which was carried out by injecting fluorescein (0.1 mL/mouse of 5% (w/v) solution) via the jugular vein, which was allowed to circulate for 30–40 sec. The cranial preparations were then exposed to stabilized mercury. Photochemically induced injury to arterioles and venules causes platelets to adhere to sites of endothelial damage and aggregation. Platelet aggregates and thrombus formation grow in size until vascular occlusion is complete. The time from injury to complete vascular occlusion (time to flow cessation) in arterioles and venules was measured in seconds. At the end of the experiment, animals were euthanized with an overdose of urethane.

In vitro Platelet Aggregation in Mouse Whole Blood

In vitro platelet aggregation in whole blood collected from BALB/c mice after i.t. instillation of saline or CuONPs was performed with slight modifications as previously described.[9,28] After anesthesia, blood from untreated mice was withdrawn from the inferior vena cava, placed in citrate (3.2%), and 0.1 mL aliquots were added to the well of a Merlin coagulometer (MC 1 VET; Merlin, Lemgo, Germany). Blood samples were incubated at 37.2°C with ADP (0.1 μM) for 3 min and then stirred for another 3 min. At the end of this period, 25-μL samples were removed and fixed on ice in 225 mL CellFix (Becton Dickinson, Franklin Lakes, NJ, USA). After fixation, single platelets were counted in a VET ABX Micros with a mouse card (ABX). The occurrence of platelet aggregation induced by ADP caused a decrease in the counted single platelets in the blood (decrease in the number of single platelets counted) obtained from the saline and CuONPs treated groups compared with each other and with untreated (without ADP) whole blood obtained from control (unexposed) mice.

Prothrombin Time (PT) and Activated Partial Thromboplastin Time (aPTT) Measurements in Plasma

PT and aPTT were measured in plasma collected from treated mice using TEClot PT-S and TEClot aPTT-S kits (TECO GmbH, Dieselstr. 1, 84088, Neufahrn, NB, Germany), according to the manufacturer's instructions. Briefly, the PT and aPTT were measured in platelet poor plasma (PPP), pre-incubated at 37°C for 3 min, followed by addition of PT and aPTT reagent using a Merlin coagulometer (MC 1 VET, Merlin, Lemgo, Germany).

Measurement of Systemic Markers of Inflammation, Coagulation and Fibrinolysis: Detection of C-Reactive Protein (CRP), Fibrinogen, Platelet Factor 4 (PF4) and Plasminogen Activator Inhibitor-1 (PAI-1)

The plasma concentrations of CRP (GenWay Biotech, Inc., San Diego, CA, USA), fibrinogen (Molecular Innovation, Southfield, MI, USA), PF4 (R&D Systems, Minneapolis, MN, USA), and PAI-1 (Molecular Innovation, Southfield, USA) were determined using an ELISA Kit.

Measurement of Proinflammatory Cytokines: Detection of Tumor Necrosis Factor Alpha (TNF-α), Interleukin 6 (IL-6) and Interleukin 1β (IL-1β) in Plasma

TNF-α, IL-6, and IL-1β levels were measured in the plasma using ELISA Kits (Duo Set, R&D Systems, Minneapolis, MN, USA), according to the manufacturer's instructions.

Oxidative Stress and Lipid Peroxidation Evaluation: Measurement of Thiobarbituric Acid Reactive Substance (TBARS), Reduced Glutathione (GSH) and Nitric Oxide (NO)

NADPH-dependent membrane lipid peroxidation was quantified in the plasma by TBARS, using malonedialdehyde as a standard (Sigma-Aldrich Fine Chemicals, St Louis, MO, USA).[29] The GSH concentration in the plasma was measured

using a commercially available kit (Sigma-Aldrich Fine Chemicals, St Louis, MO, USA). NO was measured in the plasma using a total NO assay kit from R&D Systems (Minneapolis, MN, USA), which detects the more stable NO metabolites, NO_2^- and NO_3.[−30]

Oxidative DNA Damage Evaluation by Measurement of 8-Hydroxy-2-Deoxyguanosine (8-OH-dG) in Plasma

8-OH-dG was quantified in the plasma using an ELISA kit (Cayman, Ann Arbor, MI, USA) according to the manufacturer's instruction.[9]

Estimation of Cleaved Caspase-3 and Cytochrome C in Plasma

The quantification of cleaved caspase-3 (R&D Systems, Minneapolis, MN, USA) and cytochrome C (R&D Systems, Minneapolis, MN, USA) in plasma was done using commercially available ELISA kits.

Statistics

All statistical analyses were performed using GraphPad Prism v7 (GraphPad Software Inc., San Diego, CA, USA). Data normality was assessed using the Shapiro–Wilk test. Normally distributed data were analyzed using one-way ANOVA followed by Holm–Sidak's post hoc test. Non-normal data (TNFα, IL-6, PAI-1, TBARS, and NO levels) were analyzed using the Kruskal–Wallis test, followed by Dunn's post hoc test. Results are expressed as the mean ± SEM, and statistical significance was set at $P < 0.05$.

Results

Characterization of CuONPs

Figure 1A shows the XRD pattern of the CuONPs. The diffraction peaks of the CuONPs reflect the high crystallinity of the powder compared to the standard JCPDS card no. 01-080-0076.[26] CuONPs showed sharp peaks at 2θ values of 32.8, 35.9, 39.0, 49.1, 53.8, 58.6, 61.8, 66.3, 68.3, 72.7 and 75.4, which represent the diffraction planes of the (110), (002), (111), (−202), (020), (202), (−113), (−311), (200), (311), and (−222), respectively.[27] These findings confirm the high purity of CuONPs. In contrast, Figure 1B shows that the DLS particle size distribution of CuONPs with an average size of 120.7 nm was detected. The unimodal particle size distribution of the CuONPs indicates their high homogeneity. Moreover, the CuONPs showed an average zeta potential of −17.7 mV, as demonstrated in Figure 1C). This revealed negatively charged surfaces, which were attributed to the presence of hydroxyl (–OH) groups on the surfaces of the CuONPs. This is also an indication of the electrostatic stability of the CuONPs in aqueous media under neutral pH conditions.

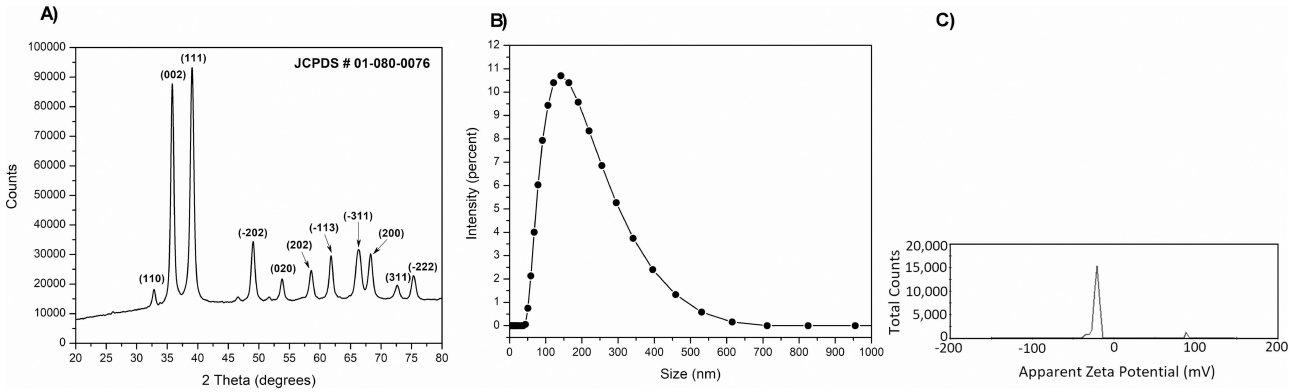

Figure 1 X-ray diffraction (XRD) pattern (**A**) of the synthesized sample showing characteristic peaks indexed to the standard JCPDS card number (#) 01-080-0076, confirming crystalline structure of copper oxide nanoparticles(CuONPs); (**B**) dynamic light scattering (DLS) size distribution indicating an average hydrodynamic diameter of 120.7 nm; and (**C**) zeta potential distribution curve showing the surface charge of the particles, demonstrating their colloidal stability in suspension.

https://doi.org/10.2147/IJN.S579331

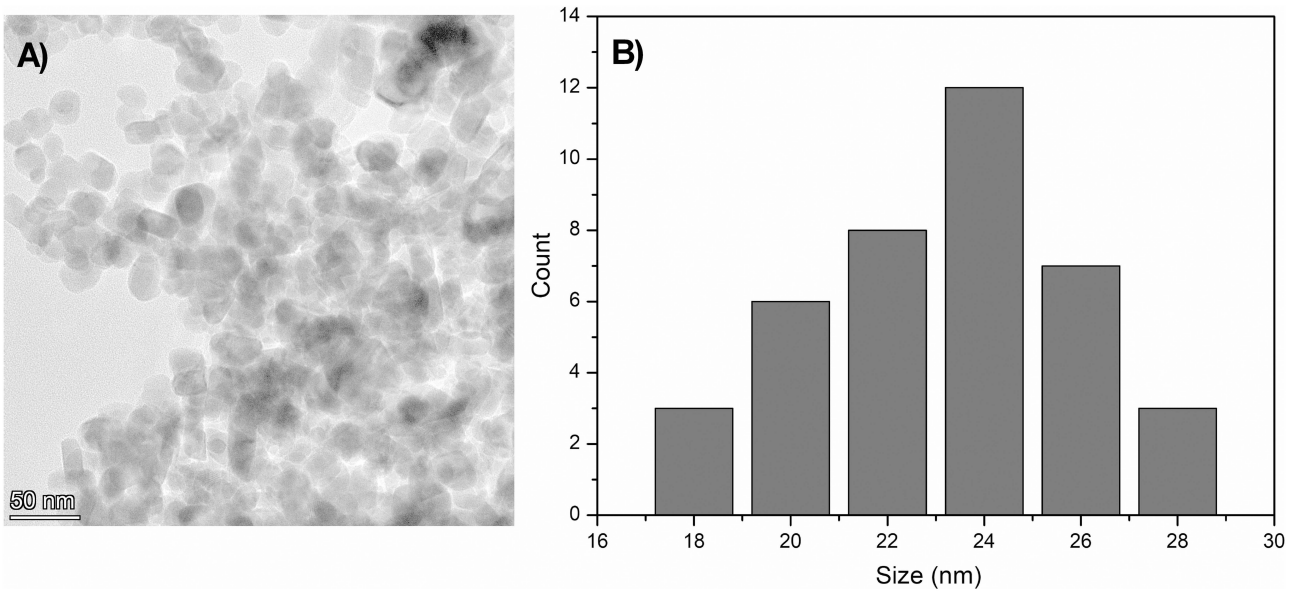

Figure 2 Transmission electron micrograph showing morphology (**A**) particle size distribution and average particle size of copper oxide nanoparticles (CuONPs, (**B**)).

Figure 2A shows the TEM micrograph of the CuONPs. All non-agglomerated NPs showed an almost round morphology with a homogeneous particle size distribution and an average particle size of 23.5 nm (Figure 2B).

Effect of CuONPs on Photochemically Induced Thrombosis in Pial Arterioles and Venules of Mouse in vivo

Figure 3 illustrates the effect of CuONPs on the thrombotic occlusion time. CuONPs induced a significant dose-dependent shortening of thrombotic occlusion time in both arterioles and venules at both tested doses. Compared with the control, significance was achieved for both doses of CuONPs ($P < 0.0001$). In addition, significant shortening was observed at higher doses (30 μg/mouse) of CuONPs, $P < 0.0001$ in arterioles and $P < 0.01$ in venules, compared to the lower dose (3 μg/mouse) of CuONPs tested.

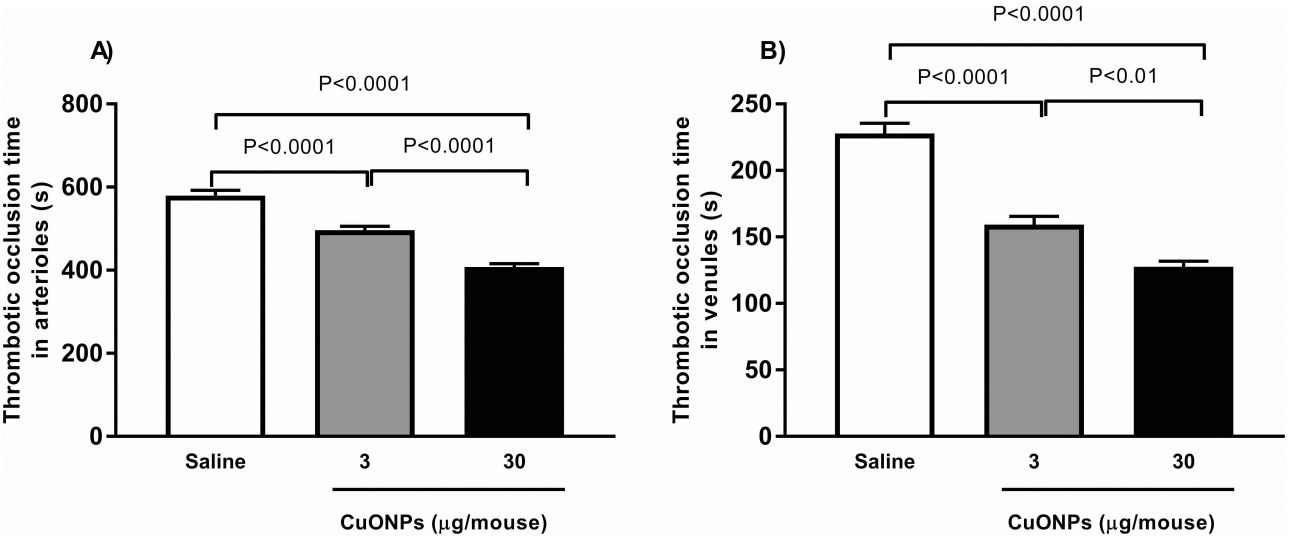

Figure 3 Thrombotic occlusion time in pial arterioles (**A**) or venules (**B**) following 24 hrs of intra-tracheal; instillation of saline (control) or copper oxide nanoparticles (CuONPs). Data are mean ± SEM (n = 8 in each group).

https://doi.org/10.2147/IJN.S579331

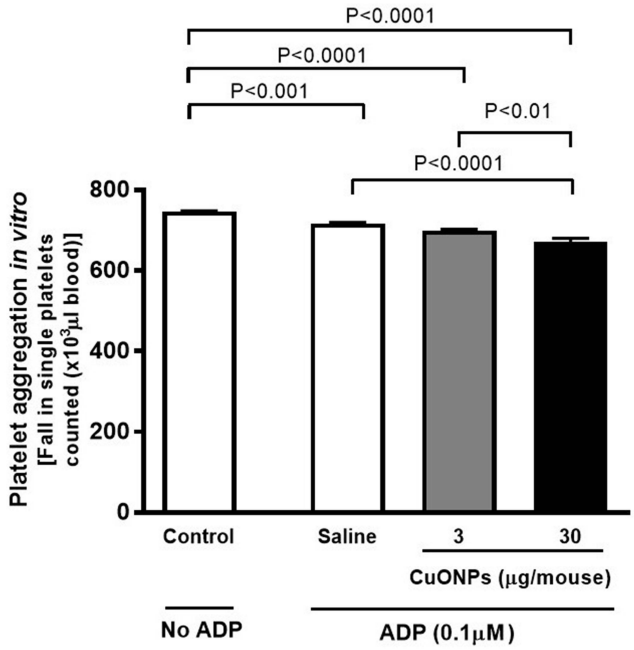

Figure 4 In vitro effect in whole blood of mice on platelet aggregation following 24 hrs of intra-tracheal instillation of saline (control) or copper oxide nanoparticles (CuONPs) in mice. Data are mean ± SEM (n = 6 in each group).

Effect of CuONPs on Platelet Aggregation in vitro

Figure 4 illustrates the effect of CuONPs on platelet aggregation in the whole blood. The in vitro ADP (0.1µM) incubation of whole blood collected from mice exposed to 30 µg CuONPs/mouse caused significant platelet aggregation compared with mice instilled with saline ($P < 0.0001$) and mice exposed to 3 µg CuONPs/mouse ($P < 0.01$).

Effect on CuONPs on PT and aPTT in vitro

Figure 5 shows the PT and aPTT in PPP collected from saline (control) or CuONPs-instilled mice. Compared to the control, a significant decrease in PT (Figure 5A) was observed in mice treated with 30 µg CuONPs/mouse ($P < 0.0001$). A similar significant decrease was also observed with aPTT (Figure 5B) in mice exposed to 30 µg CuONPs/mouse compared to the control. The level of significance was also achieved with 30 µg CuONPs compared to 3 µg CuONPs for both PT and aPTT ($P < 0.0001$).

Effect of CuONPs of Systemic Markers of Inflammation, Coagulation and Fibrinolysis

The plasma concentrations of CRP, fibrinogen, PF 4 and PAI-1 are shown in Figure 6. After 24 h of exposure, a significant increase in CRP (Figure 6A) was observed at 3 µg/mouse ($P < 0.001$) and 30 µg/mouse ($P < 0.0001$) compared to the control. Comparing between the doses, significant increase was observed at 30 µg/mouse, compared to 3 µg/mouse ($P < 0.0001$).

CuONPs significantly increased fibrinogen levels (Figure 6B) at 3 µg/mouse ($P < 0.01$) and 30 µg/mouse ($P < 0.0001$) compared with the control. Among the two doses, 30 µg/mouse showed a significant increase ($P < 0.0001$) compared to the lower dose.

A similar significant increase was observed in PF4 (Figure 6C) at 3 µg/mouse ($P < 0.01$) and 30 µg/mouse ($P < 0.0001$) compared with the control. Comparing the two doses, higher dose showed significant increase ($P < 0.01$) compared to the lower dose.

As for PAI-1 (Figure 6D), CuONPs significantly increased its concentration only at the higher dose of 30 µg/mouse ($P < 0.0001$).

https://doi.org/10.2147/IJN.S579331

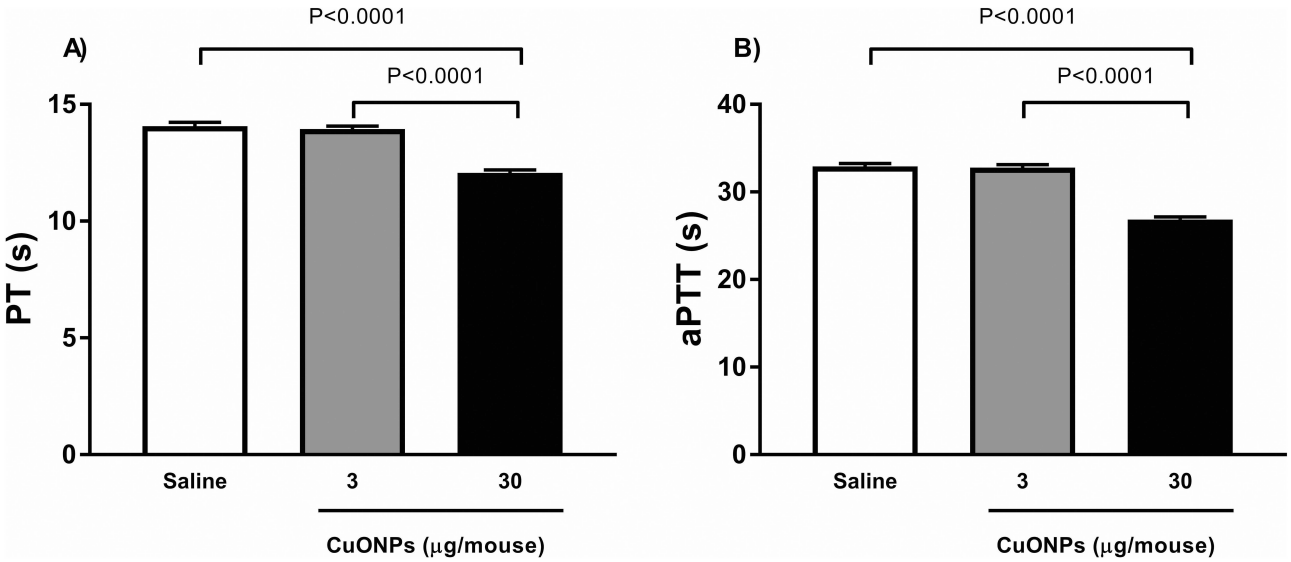

Figure 5 Prothrombin time (PT, (**A**)) and activated partial thromboplastin time (aPTT, (**B**)) measured following 24 hrs of intra-tracheal instillation of saline (control) or copper oxide nanoparticles (CuONPs) in mice. Data are mean ± SEM (n = 8 in each group).

Effect of CuONPs of Cytokines Concentrations in Plasma

The concentrations of TNF-α, IL-6, and IL-1β are shown in Figure 7. After 24 h of exposure, the administered CuONPs caused a dose-dependent increase in the levels of all the cytokines. The increase was statistically significant at 30 μg/mouse for TNF-α ($P < 0.0001$), IL-6 ($P < 0.0001$), and IL-1β ($P < 0.001$) compared with the control. A significant increase was also observed for IL-1β at 3 μg/mouse ($P < 0.01$) compared to the control.

Effect of CuONPs on Lipid Peroxidation and Oxidative Stress Markers

The TBARS, GSH, and NO levels following exposure to CuONPs are shown in Figure 8. After 24 h of exposure, a dose-dependent increase in TBARS (Figure 8A) was observed for CuONPs. The level of significance was achieved at 30 μg/mouse compared with both the control ($P < 0.0001$) and 3 μg/mouse ($P < 0.05$). Compared with the control group, CuONPs caused a dose-dependent decrease in GSH (Figure 8B) at 3 μg/mouse and 30 μg/mouse ($P < 0.0001$ for both). A significant decrease was also observed at 30 μg/mouse ($P < 0.0001$) compared to that at 3 μg/mouse. A dose-dependent decrease in NO (Figure 8C) was also observed in CuONPs-exposed mice compared with that in the control. However, the level of significance was only observed at the dose of 30 μg/mouse ($P < 0.0001$).

Effect of CuONPs on Oxidative DNA Damage

Figure 9 shows the concentration of 8-OH-dG in the plasma 24 h after i.t. instillation of either saline or CuONPs. After 24 h of exposure, the level of 8-OH-dG significantly increased in a dose-dependent manner in the CuONPs-treated group ($P < 0.0001$ for both) compared with the control. The level of significance was also achieved at 30 μg/mouse ($P < 0.001$) compared to 3 μg/mouse.

Effect of CuONPs on Markers of Apoptosis

Figure 10 illustrates the levels of cleaved caspase-3 and cytochrome C in the plasma of either saline- or CuONPs-instilled mice. A significant dose-dependent increase in cleaved caspase-3 was observed 3 μg/mouse and 30 μg/mouse ($P < 0.0001$ for both) compared with that in the control. A significant dose-dependent increase in cytochrome C was also observed at 3 μg/mouse ($P < 0.001$) and 30 μg/mouse ($P < 0.0001$) compared to the control. For both cleaved caspase-3 and cytochrome C, the level of significance was also higher at 30 μg/mouse ($P < 0.0001$) than at 3 μg/mouse.

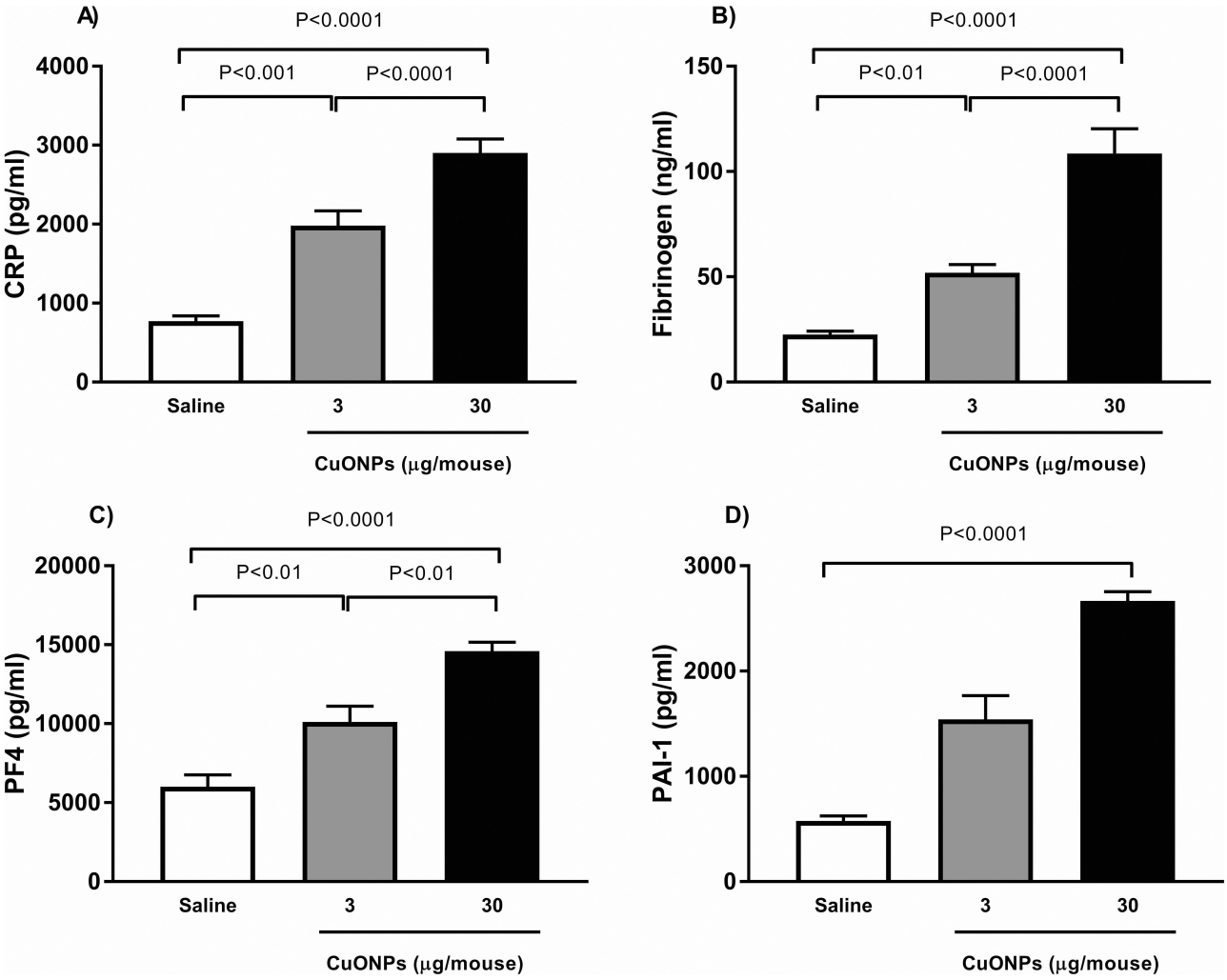

Figure 6 C-reactive protein (CRP, (**A**)), fibrinogen (**B**), Platelet factor 4 (PF4, (**C**)) and Plasminogen activator inhibitor-1 (PAI-1, (**D**)) concentrations in plasma following 24 hrs of intra-tracheal instillation of saline (control) or copper oxide nanoparticles (CuONPs) in mice. Data are mean ± SEM (n = 8 in each group).

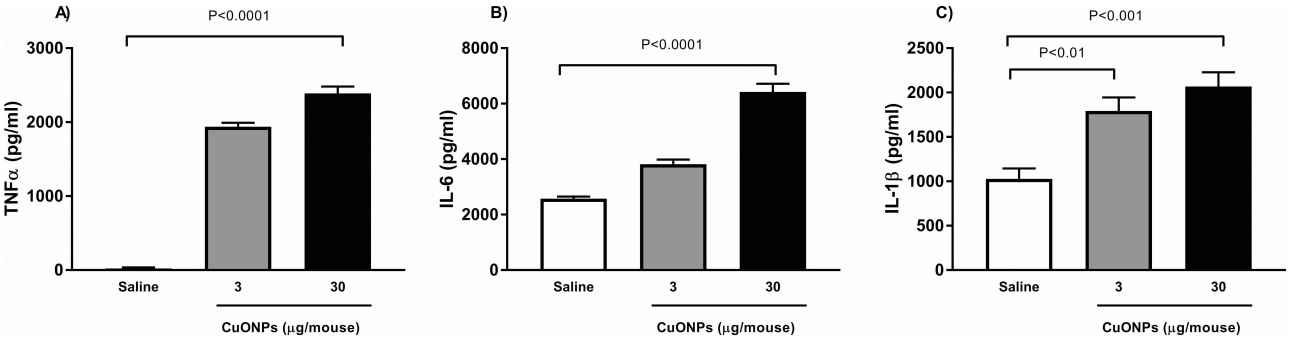

Figure 7 Tumor necrosis factor α (TNF α, (**A**)), interleukin-6, (IL-6, (**B**)), and IL-1β (**C**) in plasma following 24 hrs of intra-tracheal instillation of saline (control) or copper oxide nanoparticles (CuONPs) in mice. Data are mean ± SEM (n = 8 in each group).

Discussion

In the present study, we evaluated the systemic effect 24 h after a single i.t. instillation of 3 μg/mouse or 30 μg/mouse CuONPs. Our findings revealed that CuONPs can induce acute dose-dependent systemic effects including thrombosis, inflammation, oxidative stress, DNA damage, and apoptosis.

https://doi.org/10.2147/IJN.S579331

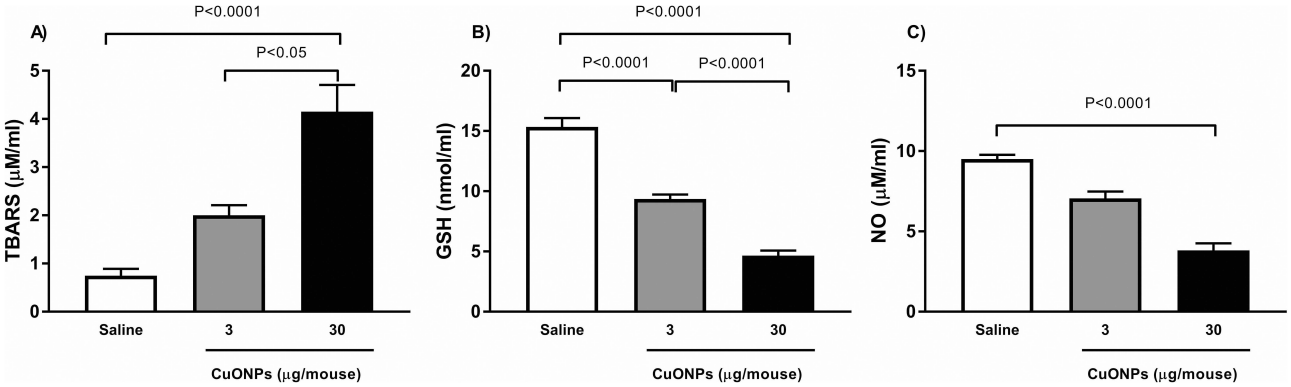

Figure 8 TBARS (**A**), reduced glutathione (GSH, (**B**)) and nitric oxide (NO, (**C**)) levels in plasma following 24 hrs of intra-tracheal instillation of saline (control) or copper oxide nanoparticles (CuONPs) in mice. Data are mean ± SEM (n = 8 in each group).

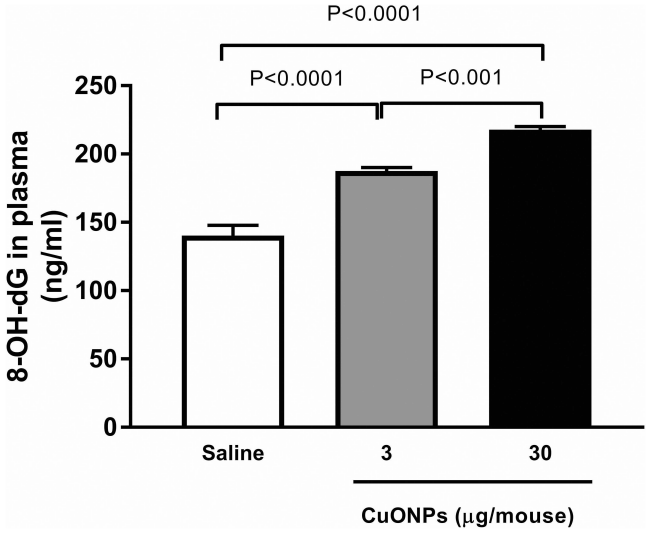

Figure 9 8-hydroxy-2-deoxyguanosine (8-OH-dG) levels in plasma following 24 hrs of intra-tracheal instillation of saline (control) or copper oxide nanoparticles (CuONPs) in mice. Data are mean ± SEM (n = 8 in each group).

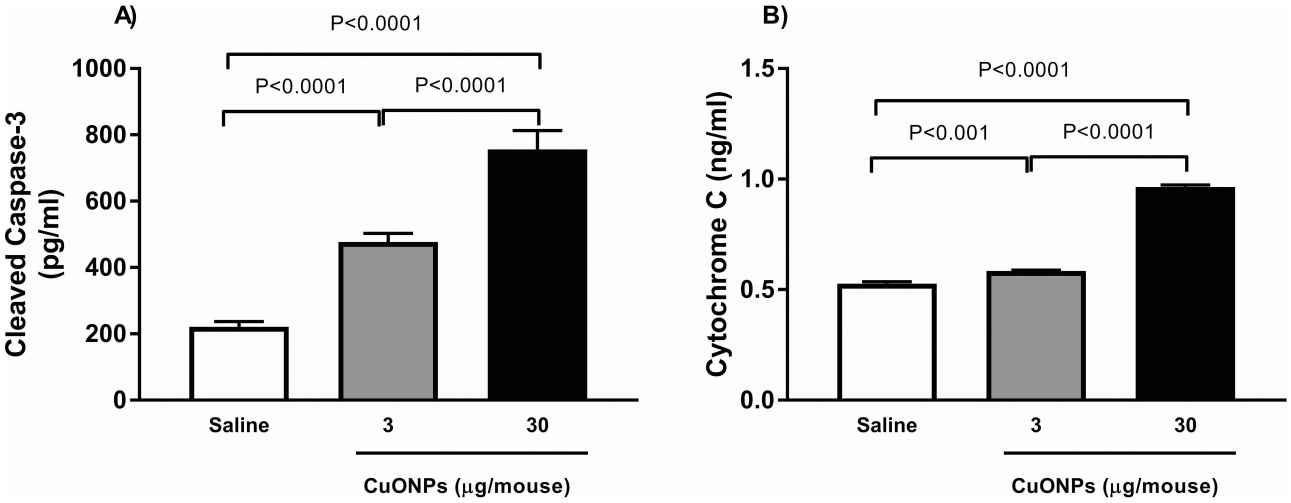

Figure 10 Cleaved caspase-3 (**A**) and cytochrome C (**B**) levels in plasma following 24 hrs of intra-tracheal instillation of saline (control) or copper oxide nanoparticles (CuONPs) in mice. Data are mean ± SEM (n = 8 in each group).

The CuONPs used in present study were comprehensively characterized using XRD, DLS, zeta potential analyses and TEM to evaluate their structural and colloidal properties. The XRD pattern exhibits distinct and sharp diffraction peaks corresponding to monoclinic CuO (JCPDS 01-080-0076), confirming the high crystallinity and phase purity of the nanoparticles. DLS analysis revealed a relatively uniform particle size distribution with an average hydrodynamic diameter of 120.7 nm, which is larger than the 15–50 nm range reported by the manufacturer. This is further supported by TEM analysis, which shows that non-agglomerated nanoparticles exhibit an almost spherical morphology with an average particle size of 23.5 nm. Furthermore, the zeta potential value of −17.7 mV demonstrated good electrostatic stability, suggesting sufficient surface charge to minimize aggregation. Collectively, these results confirm that the obtained CuONPs possess high crystallinity, good electrostatic stability, and a consistent nanoscale distribution suitable for subsequent experimental applications.

I.t. instillation was selected as the mode of CuONPs delivery in this study because mice are obligate nose breathers and provide controlled, localized, and reproducible means of introducing nanoparticles directly into the lower respiratory tract. This method bypasses the variability associated with inhalation exposure systems while ensuring that a precise and uniform dose reaches the pulmonary region, allowing for a more accurate assessment of nanoparticle-induced biological effects. Moreover, i.t. instillation is widely used in toxicological studies to investigate systemic responses to particulate matter and engineered nanomaterials, making it a well-established approach for mechanistic evaluation.[9,28,31]

CuONPs (3 μg/mouse and 30 μg/mouse) were selected to represent the low- and high-exposure scenarios, respectively, within a biologically relevant range. Previous studies using CuONPs via i.t. instillation have adopted similar dosing schemes; for example, doses of 3, 35, and 100 μg/mouse have been employed to assess pulmonary infection defenses and systemic responses in mice.[32] Moreover, doses of 30, 50, and 100 μg/mouse have been used in neurotoxicity studies, demonstrating clear dose-dependent effects on oxidative stress and histopathology in the brain following pulmonary administration.[33] Thus, our selected dose levels provide a meaningful framework for understanding the pulmonary and systemic effects of CuONPs exposure.

Over the past decade, numerous studies and reviews have highlighted the potential toxicity of metal-oxide nanoparticles, including their hemocompatibility and cardiovascular effects.[34–37] Platelets, key cellular components of the blood, play a central role in hemostasis and thrombosis. Under normal physiological conditions, circulating platelets do not adhere to microvascular endothelium. However, upon vascular injury, platelet adhesion, aggregation, and subsequent thrombus formation occur in both venules and arterioles in vivo. The thrombotic occlusion time in these vessels is widely used in experimental research as an indicator of blood coagulation status because it reflects the kinetics of thrombus formation in response to a prothrombotic stimulus.[28,38] Shortened occlusion times were indicative of a hypercoagulable state, whereas prolonged times were indicative of hypocoagulability. In the present study, we observed a significant reduction in thrombotic occlusion time in CuONPs-instilled mice compared with controls, demonstrating the prothrombotic potential of the tested nanoparticles. These findings are consistent with our previous investigations on silver nanoparticles (AgNPs), diesel exhaust particles, and cerium oxide nanoparticles.[9,28,38–40] Importantly, unlike our earlier work, the current study specifically evaluates CuONPs, which have distinct physicochemical and biological characteristics, thereby extending our research into a different and previously unexamined class of metal-oxide nanoparticles. To further elucidate the mechanisms underlying the prothrombotic effects of CuONPs, we examined in vitro platelet aggregation in whole blood, as well as coagulation pathway activation. Similar to previous studies, the addition of ADP to the whole blood of CuONPs-exposed mice induced significant platelet aggregation, with a more pronounced effect observed at a higher dose (30 μg/mouse). In addition, we observed shortening of both the PT and aPTT pathways in response to CuONPs exposure compared with the controls. Taken together, these findings indicate that CuONPs exposure promotes a hypercoagulable state. We further studied the effects of CuONPs on hemostatic markers, including fibrinogen, PAI-1, PF4, and CRP. The significant increase in these markers collectively supports the interpretation that CuONPs exposure promotes a prothrombotic state.[41–44] Elevated PF4 levels indicate heightened platelet activation and degranulation, which are the key initiating steps in thrombus formation.[43] Increased fibrinogen not only reflects systemic inflammation but also enhances clot formation by serving as a substrate for fibrin, thereby facilitating platelet aggregation and stabilizing thrombi.[41] Elevated PAI-1 levels suggest impaired fibrinolysis, as inhibition of plasminogen activators reduces clot breakdown and prolongs thrombus persistence.[42] Finally, increased CRP levels confirmed systemic

inflammation, which was closely linked to endothelial activation and a procoagulant shift in vascular homeostasis.[44] Together, these biomarkers demonstrate the convergence of platelet activation, coagulation cascade amplification, fibrinolytic inhibition, and inflammation, providing strong mechanistic evidence that CuONPs induce hypercoagulability and increase the risk of thrombosis.

Our evaluation of proinflammatory cytokines revealed significant increases in TNF-α, IL-6, and IL-1β levels following pulmonary instillation of CuONPs compared with saline-treated controls. This elevation may result from a robust local inflammatory response in the lung, which subsequently spills into the systemic circulation, or from the direct translocation of nanoparticles across the air–blood barrier.[45] The upregulation of these cytokines indicates that CuONPs trigger pulmonary inflammation, which in turn likely contributes to systemic effects such as endothelial activation and dysfunction, elevated acute-phase protein levels, and enhanced platelet activation with subsequent coagulation cascade stimulation.

In parallel, pulmonary exposure to CuONPs resulted in significantly increased TBARS levels along with decreased levels of NO and reduced GSH. TBARS is a well-established marker of lipid peroxidation, reflecting enhanced oxidative stress and membrane damage, whereas GSH serves as a critical intracellular antioxidant, and its depletion indicates impaired redox defense capacity.[46,47] Reduced NO bioavailability is particularly relevant in the vascular context because NO normally exerts vasodilatory, anti-inflammatory, and antithrombotic effects, and its suppression favors endothelial dysfunction, platelet activation, and vascular inflammation.[47] Together, these alterations in oxidative stress markers support our interpretation that CuONPs induce a systemic pro-oxidant environment that amplifies both prothrombotic and proinflammatory responses observed in our study. Consistent with our findings, previous studies have shown that CuONPs elevate lipid peroxidation and deplete antioxidant defenses in the liver and kidney and that nanoparticle-induced oxidative stress can impair NO signaling, thereby promoting platelet hyperreactivity and thrombosis.[47–50] These results collectively suggest that oxidative stress is a central mechanism linking CuONPs exposure to vascular and inflammatory dysfunctions.

We further examined the effects of CuONPs on DNA damage and apoptosis and observed significant increases in 8-OH-dG, cleaved caspase-3, and cytochrome C. Similar responses were noted in our previous studies investigating the pathophysiological effects of pulmonary exposure to AgNPs and cerium oxide nanoparticles.[9,11,40] 8-OH-dG is a well-established biomarker of oxidative DNA damage, formed by the hydroxyl radical–mediated oxidation of guanine bases; elevated levels indicate heightened ROS activity and compromised genomic stability.[51] Caspases are the key mediators of apoptosis. Cleaved caspase-3 functions as a critical executioner of apoptosis, marking the progression of programmed cell death, often in response to mitochondrial dysfunction or excessive ROS.[52] Cytochrome C release from the mitochondria into the cytosol is a defining feature of the intrinsic apoptotic pathway, linking oxidative mitochondrial injury to downstream caspase activation.[53] Together, the increased levels of 8-OH-dG, cytochrome C, and cleaved caspase-3 in CuONPs-exposed mice corroborate earlier findings of disrupted redox balance and demonstrate that oxidative insults extend beyond lipids and proteins to encompass DNA damage, mitochondrial dysfunction, and activation of apoptotic cascades.

Conclusion

Our study provides a comprehensive assessment of CuONPs 24 h after i.t. instillation, using both in vivo and in vitro models. We observed acute systemic toxicity, including oxidative stress, inflammation, DNA damage, apoptosis, and enhanced thrombotic responses, with more pronounced effects observed at higher doses. Although limited by a single exposure route, only two doses, a narrow size range, and short-term evaluation, our findings consistently indicate that CuONPs can induce systemic effects beyond the site of deposition. These results underscore the need for further investigation with varied exposure routes, dosing regimens, and long-term assessments to fully delineate the pathophysiological effects of CuONPs. Importantly, our data highlight the necessity for caution in their biomedical and industrial use given their potential to trigger proinflammatory and prothrombotic responses.

Funding

This work was supported by funds from the United Arab Emirates University, Zayed Bin Sultan Center of Health Sciences (grant#12R267).

Disclosure

The authors report no conflicts of interest in this work.

References

1. Nikalje AP. Nanotechnology and its applications in medicine. *Med Chem*. 2015;5(2):081–089. doi:10.4172/2161-0444.1000247
2. Vance ME, Kuiken T, Vejerano EP, et al. Nanotechnology in the real world: redeveloping the nanomaterial consumer products inventory. *Beilstein J Nanotechnol*. 2015;6(1):1769–1780. doi:10.3762/bjnano.6.181
3. Pathakoti K, Goodla L, Manubolu M, Hwang H-M. Nanoparticles and their potential applications in agriculture, biological therapies, food, biomedical, and pharmaceutical industry: a review. In: *Nanotechnology and Nanomaterial Applications in Food, Health, and Biomedical Sciences*. 2019:121–162.
4. Bhattacharya PT, Misra SR, Hussain M. Nutritional aspects of essential trace elements in oral health and disease: an extensive review. *Scientifica*. 2016;2016(1):5464373. doi:10.1155/2016/5464373
5. Ameh T, Sayes CM. The potential exposure and hazards of copper nanoparticles: a review. *Environ Toxicol Pharmacol*. 2019;71:103220. doi:10.1016/j.etap.2019.103220
6. Chibber S, Shanker R. Can CuO nanoparticles lead to epigenetic regulation of antioxidant enzyme system? *J Appl Toxicol*. 2017;37(1):84–91. doi:10.1002/jat.3392
7. Santhosh G, Nayaka GP. Nanoparticles in construction industry and their toxicity. In: *Ecological and Health Effects of Building Materials*. Springer; 2021:133–146.
8. Wiemann M, Vennemann A, Blaske F, Sperling M, Karst U. Silver nanoparticles in the lung: toxic effects and focal accumulation of silver in remote organs. *Nanomaterials*. 2017;7(12):441. doi:10.3390/nano7120441
9. Ferdous Z, Al-Salam S, Greish YE, Ali BH, Nemmar A. Pulmonary exposure to silver nanoparticles impairs cardiovascular homeostasis: effects of coating, dose and time. *Toxicol Appl Pharmacol*. 2019;367:36–50. doi:10.1016/j.taap.2019.01.006
10. Nemmar A, Al-Salam S, Al Ansari Z, et al. Impact of pulmonary exposure to cerium oxide nanoparticles on experimental acute kidney injury. *Cell Physiol Biochem*. 2019;52(3):439–454.
11. Nemmar A, Yuvaraju P, Beegam S, Fahim MA, Ali BH. Cerium oxide nanoparticles in lung acutely induce oxidative stress, inflammation, and DNA damage in various organs of mice. *Oxid Med Cell Longev*. 2017;2017(1):9639035. doi:10.1155/2017/9639035
12. Sajjad H, Sajjad A, Haya RT, Khan MM, Zia M. Copper oxide nanoparticles: in vitro and in vivo toxicity, mechanisms of action and factors influencing their toxicology. *Comp Biochem Physiol C Toxicol Pharmacol*. 2023;271:109682. doi:10.1016/j.cbpc.2023.109682
13. Perreault F, Melegari SP, da Costa CH, Rossetto A, Popovic R, Matias WG. Genotoxic effects of copper oxide nanoparticles in Neuro 2A cell cultures. *Sci Total Envir*. 2012;441:117–124. doi:10.1016/j.scitotenv.2012.09.065
14. Ahamed M, Siddiqui MA, Akhtar MJ, Ahmad I, Pant AB, Alhadlaq HA. Genotoxic potential of copper oxide nanoparticles in human lung epithelial cells. *Biochem Biophys Res Commun*. 2010;396(2):578–583. doi:10.1016/j.bbrc.2010.04.156
15. Piret J-P, Jacques D, Audinot J-N, et al. Copper (II) oxide nanoparticles penetrate into HepG2 cells, exert cytotoxicity via oxidative stress and induce pro-inflammatory response. *Nanoscale*. 2012;4(22):7168–7184. doi:10.1039/c2nr31785k
16. Rodhe Y, Skoglund S, Wallinder IO, Potácová Z, Möller L. Copper-based nanoparticles induce high toxicity in leukemic HL60 cells. *Toxicol In vitro*. 2015;29(7):1711–1719. doi:10.1016/j.tiv.2015.05.020
17. Sun Y, Zhang G, He Z, Wang Y, Cui J, Li Y. Effects of copper oxide nanoparticles on developing zebrafish embryos and larvae. *Int J Nanomed*. 2016;11:905–918. doi:10.2147/IJN.S100350
18. Mashock MJ, Zanon T, Kappell AD, Petrella LN, Andersen EC, Hristova KR. Copper oxide nanoparticles impact several toxicological endpoints and cause neurodegeneration in Caenorhabditis elegans. *PLoS One*. 2016;11(12):e0167613. doi:10.1371/journal.pone.0167613
19. Zhang X, Peng Z, Wang Q, Zhang W, Bu Q, Sun D. Copper oxide nanoparticles induce pulmonary inflammation via triggering cellular cuproptosis. *Toxicology*. 2025;514:154131. doi:10.1016/j.tox.2025.154131
20. Lai X, Zhao H, Zhang Y, et al. Intranasal delivery of copper oxide nanoparticles induces pulmonary toxicity and fibrosis in C57BL/6 mice. *Sci Rep*. 2018;8(1):4499. doi:10.1038/s41598-018-22556-7
21. Areecheewakul S, Adamcakova-Dodd A, Haque E, et al. Time course of pulmonary inflammation and trace element biodistribution during and after sub-acute inhalation exposure to copper oxide nanoparticles in a murine model. *Part Fibre Toxicol*. 2022;19(1):40. doi:10.1186/s12989-022-00480-z
22. Cojocaru E, Petriș OR, Cojocaru C. Nanoparticle-based drug delivery systems in inhaled therapy: improving respiratory medicine. *Pharmaceuticals*. 2024;17(8):1059. doi:10.3390/ph17081059
23. Abdelkareem S, El-Sayed MMH, Yacoub N, et al. Copper oxide nanoparticles as delivery vehicles for different Pt(ii)-drugs: experimental and theoretical evaluation. *J Mat Chem B*. 2025;13(32):10027–10042. doi:10.1039/D4TB02636E
24. Naz S, Gul A, Zia M. Toxicity of copper oxide nanoparticles: a review study. *IET Nanobiotechnol*. 2020;14(1):1–13. doi:10.1049/iet-nbt.2019.0176
25. Guo L-M, Xu X-M, Zhao D, Cai X-G, Zhou B. Biosynthesis, characterization of PLGA coated folate-mediated multiple drug loaded copper oxide (CuO) nanoparticles and it's cytotoxicity on nasopharyngeal cancer cell lines. *AMB Express*. 2020;10(1):160. doi:10.1186/s13568-020-01096-2
26. Nagajyothi PC, Muthuraman P, Sreekanth TVM, Kim DH, Shim J. Green synthesis: in-vitro anticancer activity of copper oxide nanoparticles against human cervical carcinoma cells. *Arabian J Chem*. 2017;10(2):215–225. doi:10.1016/j.arabjc.2016.01.011
27. Veisi H, Karmakar B, Tamoradi T, Hemmati S, Hekmati M, Hamelian M. Biosynthesis of CuO nanoparticles using aqueous extract of herbal tea (Stachys Lavandulifolia) flowers and evaluation of its catalytic activity. *Sci Rep*. 2021;11(1):1983. doi:10.1038/s41598-021-81320-6

28. Nemmar A, Al-Salam S, Beegam S, Yuvaraju P, Ali BH. The acute pulmonary and thrombotic effects of cerium oxide nanoparticles after intratracheal instillation in mice. *Int J Nanomed*. 2017;12:2913. doi:10.2147/IJN.S127180
29. Nemmar A, Al-Salam S, Yuvaraju P, Beegam S, Ali BH. Emodin mitigates diesel exhaust particles-induced increase in airway resistance, inflammation and oxidative stress in mice. *Respir Physiol Neurobiol*. 2015;215:51–57. doi:10.1016/j.resp.2015.05.006
30. Tsikas D. Review Methods of quantitative analysis of the nitric oxide metabolites nitrite and nitrate in human biological fluids. *Free Radical Res*. 2005;39(8):797–815. doi:10.1080/10715760500053651
31. Xiao J, Tu B, Zhou X, et al. Autophagy deficiency exacerbates acute lung injury induced by copper oxide nanoparticles. *J Nanobiotechnol*. 2021;19 (1):162. doi:10.1186/s12951-021-00909-1
32. Kim JS, Adamcakova-Dodd A, O'Shaughnessy PT, Grassian VH, Thorne PS. Effects of copper nanoparticle exposure on host defense in a murine pulmonary infection model. *Part Fibre Toxicol*. 2011;8(1):29. doi:10.1186/1743-8977-8-29
33. Zhou H, Yao L, Jiang X, et al. Pulmonary exposure to copper oxide nanoparticles leads to neurotoxicity via oxidative damage and mitochondrial dysfunction. *Neurotox Res*. 2021;39(4):1160–1170. doi:10.1007/s12640-021-00358-6
34. Sengul AB, Asmatulu E. Toxicity of metal and metal oxide nanoparticles: a review. *Environ Chem Lett*. 2020;18(5):1659–1683. doi:10.1007/s10311-020-01033-6
35. Nagarajan M, Maadurshni GB, Tharani GK, et al. Exposure to zinc oxide nanoparticles (ZnO-NPs) induces cardiovascular toxicity and exacerbates pathogenesis–Role of oxidative stress and MAPK signaling. *Chem Biol Interact*. 2022;351:109719. doi:10.1016/j.cbi.2021.109719
36. Líšková S, Bališ P, Mičurová A, et al. Effect of iron oxide nanoparticles on vascular function and nitric oxide production in acute stress-exposed rats. *Physiol Res*. 2020;69(6):1067. doi:10.33549/physiolres.934567
37. Eldine RSS, Shalaby TI, Balbaa OA. Evaluation of toxicity of copper oxide nano particles on human blood. *J Biophys Struct Biol*. 2021;9(1):10–19.
38. Ferdous Z, Beegam S, Zaaba NE, et al. Exacerbation of thrombotic responses to silver nanoparticles in hypertensive mouse model. *Oxid Med Cell Longev*. 2022;2022:2079630. doi:10.1155/2022/2079630
39. Nemmar A, Al-Maskari S, Ali BH, Al-Amri IS. Cardiovascular and lung inflammatory effects induced by systemically administered diesel exhaust particles in rats. *Am J Physiol Lung Cell Mol Physiol*. 2007;292(3):L664–L670. doi:10.1152/ajplung.00240.2006
40. Ferdous Z. *Pulmonary and Sytemic Pathophysiological Impact of Silver Nanoparticles: Effects of Coating, Time, and Dose*. Doctoral Dissertation. United Arab Emirates University; 2020.
41. Kattula S, Byrnes JR, Wolberg AS. Fibrinogen and fibrin in hemostasis and thrombosis. *Arterioscler Thromb Vasc Biol*. 2017;37(3):e13–e21. doi:10.1161/ATVBAHA.117.308564
42. Cesari M, Pahor M, Incalzi RA. Plasminogen activator inhibitor-1 (PAI-1): a key factor linking fibrinolysis and age-related subclinical and clinical conditions. *Cardiovasc Ther*. 2010;28(5):e72–e91. doi:10.1111/j.1755-5922.2010.00171.x
43. Kowalska MA, Rauova L, Poncz M. Role of the platelet chemokine platelet factor 4 (PF4) in hemostasis and thrombosis. *Thrombosis Res*. 2010;125(4):292–296. doi:10.1016/j.thromres.2009.11.023
44. Fay WP. Linking inflammation and thrombosis: role of C-reactive protein. *World J Cardiol*. 2010;2(11):365. doi:10.4330/wjc.v2.i11.365
45. Gehr P. Interaction of nanoparticles with biological systems. *Colloids Surf B*. 2018;172:395–399. doi:10.1016/j.colsurfb.2018.08.023
46. Yoshida Y, Umeno A, Shichiri M. Lipid peroxidation biomarkers for evaluating oxidative stress and assessing antioxidant capacity in vivo. *J Clin Biochem Nutr*. 2013;52(1):9–16. doi:10.3164/jcbn.12-112
47. Manke A, Wang L, Rojanasakul Y. Mechanisms of nanoparticle-induced oxidative stress and toxicity. *Biomed Res Int*. 2013;2013(1):942916. doi:10.1155/2013/942916
48. Anreddy RNR. Copper oxide nanoparticles induces oxidative stress and liver toxicity in rats following oral exposure. *Toxicol Rep*. 2018;5:903–904. doi:10.1016/j.toxrep.2018.08.022
49. Reddy ARN, Lonkala S. In vitro evaluation of copper oxide nanoparticle-induced cytotoxicity and oxidative stress using human embryonic kidney cells. *Toxicol Ind Health*. 2019;35(2):159–164. doi:10.1177/0748233718819371
50. Lei R, Yang B, Wu C, Liao M, Ding R, Wang Q. Mitochondrial dysfunction and oxidative damage in the liver and kidney of rats following exposure to copper nanoparticles for five consecutive days. *Toxicology Res*. 2015;4(2):351–364. doi:10.1039/C4TX00156G
51. Valavanidis A, Vlachogianni T, Fiotakis C. 8-hydroxy-2′-deoxyguanosine (8-OHdG): a critical biomarker of oxidative stress and carcinogenesis. *J Environ Sci Health C*. 2009;27(2):120–139. doi:10.1080/10590500902885684
52. Savitskaya MA, Onishchenko GE. Mechanisms of apoptosis. *Biochem Moscow*. 2015;80(11):1393–1405. doi:10.1134/S0006297915110012
53. Eleftheriadis T, Pissas G, Liakopoulos V, Stefanidis I. Cytochrome c as a potentially clinical useful marker of mitochondrial and cellular damage. *Front Immunol*. 2016;7:279. doi:10.3389/fimmu.2016.00279